IOPscience iopscience.iop.org

Home Search Collections Journals About Contact us My IOPscience

Structural evolution behavior of manganese monophosphide under high pressure: experimental and theoretical study

This content has been downloaded from IOPscience. Please scroll down to see the full text.

2017 J. Phys.: Condens. Matter 29 254002

(http://iopscience.iop.org/0953-8984/29/25/254002)

View the table of contents for this issue, or go to the journal homepage for more

Download details:

IP Address: 159.226.37.138
This content was downloaded on 19/07/2017 at 00:00

Please note that terms and conditions apply.

You may also be interested in:

Experimental and theoretical study of –Eu2(MoO4)3 under compression
C Guzmán-Afonso, S F León-Luis, J A Sans et al.

ScVO4 under non-hydrostatic compression: a new metastable polymorph
Alka B Garg, D Errandonea, P Rodríguez-Hernández et al.

Electronic band structures of NiAs-type compounds. I. Nonmagnetic state
K Motizuki, K Katoh and A Yanase

Structural and optical investigations of Fe1.03Se0.5Te0.5 under high pressure
Pallavi S Malavi, S Karmakar, N N Patel et al.

Pressure effects on two superconducting iron-based families
Athena S Sefat

First-principles calculations of the magnetic and electronic structures of MnP under pressure
Yuanji Xu, Min Liu, Ping Zheng et al.

Structural study of alpha-Bi2O3 under pressure
A L J Pereira, D Errandonea, A Beltrán et al.

Pressure-induced phase transitions of MnTe
M Mimasaka, I Sakamoto, K Murata et al.

Equation of state of zircon- and scheelite-type dysprosium orthovanadates: a combined experimental and theoretical study
Wojciech Paszkowicz, Olga Ermakova, Javier López-Solano et al.

IOP Publishing Journal of Physics: Condensed Matter

J. Phys.: Condens. Matter **29** (2017) 254002 (8pp) https://doi.org/10.1088/1361-648X/aa6554

Structural evolution behavior of manganese monophosphide under high pressure: experimental and theoretical study

Zhenhai Yu[1,9], Wei Wu[2,9], Pengchao Lu[6,7], Jinggeng Zhao[3], Jinguang Cheng[2,4], Qingyang Hu[1], Ye Yuan[1], Xin Li[1], Cuiying Pei[1], Fengjiao Chen[1], Zhipeng Yan[1], Shuai Yan[5], Ke Yang[5], Jian Sun[6,7,10], Jianlin Luo[2,8] and Lin Wang[1,10]

[1] Center for High Pressure Science and Technology Advanced Research, Shanghai, 201203, People's Republic of China
[2] Beijing National Lab for Condensed Matter Physics, Institute of Physics, Chinese Academy of Sciences, Beijing 100190, People's Republic of China
[3] Department of Physics, and Academy of Fundamental and Interdisciplinary Sciences, Harbin Institute of Technology, Harbin 150080, People's Republic of China
[4] School of Physical Sciences, University of Chinese Academy of Sciences, Beijing 100049, People's Republic of China
[5] Shanghai Institute of Applied Physics, Chinese Academy of Sciences, Shanghai 201203, People's Republic of China
[6] National Laboratory of Solid State Microstructures, School of Physics, Nanjing University, Nanjing 210093, People's Republic of China
[7] Collaborative Innovation Center of Advanced Microstructures, Nanjing University, Nanjing 210093, People's Republic of China
[8] Collaborative Innovation Center of Quantum Matter, Beijing, People's Republic of China

E-mail: wanglin@hpstar.ac.cn and jiansun@nju.edu.cn

Received 28 November 2016, revised 27 February 2017
Accepted for publication 8 March 2017
Published 24 May 2017

Abstract

The influence of external pressure on the structural properties of manganese monophosphides (MnP) at room temperature has been studied using *in situ* angle dispersive synchrotron x-ray powder diffraction (AD-XRD) with a diamond anvil cell. The crystal structure of MnP is stable between 0 to 15 GPa. However, the compressibility of *b*-axis is much larger than those of *a*- and *c*-axes. From this result we suggested that the occurrence of superconductivity in MnP was induced by suppression of the long-range antiferromagnetically ordered state rather than a structural phase transition. Furthermore, the present experimental results show that the *Pnma* phase of MnP undergoes a pressure-induced structural phase transition at ~15.0 GPa. This finding lighted up-to-date understanding of the common prototype B31 structure (Strukturbericht Designation: B31) in transition metal monophosphides. No additional structural phase transition was observed up to 35.1 GPa (Run 1) and 40.2 GPa (Run 2) from the present AD-XRD results. With an extensive crystal structure searching and *ab initio* calculations, we predict that MnP underwent two pressure-induced structural phase transitions of $Pnma \rightarrow P2_13$ and $P2_13 \rightarrow Pm\text{-}3m$ (CsCl-type) at 55.0 and 92.0 GPa, respectively. The structural stability and the electronic structures of manganese monophosphides under high pressure are also briefly discussed.

---

[9] These authors contributed equally to this study and share first authorship.
[10] Author to whom any correspondence should be addressed.

1361-648X/17/254002+8$33.00

Keywords: manganese-based superconductor, high-pressure effects, phase transitions

(Some figures may appear in colour only in the online journal)

1. Introduction

Recently discovered novel iron- and chromium-based superconductors have stimulated theoretical and experimental attempts to explore superconductivity in isomorphic compounds [1–3]. MnP-type (Strukturbericht designation, B31) structure was initially proposed by Hägg and Fylking [4, 5] to investigate the crystal structure of isomorphous transition metal phosphides and arsenides such as MnP and FeAs. Since then, considerable experimental efforts have been devoted to investigating the crystallographic structure in many compounds which are isomorphic to MnP. Manganese pnictides MnPn (Pn = P, As, Sb, Bi) have attracted significant interest because of their various magnetic and structural properties, such as uniaxial magnetic anisotropy and structural phase transitions [6, 7]. Recently, the interest in MnPn compounds has been strongly enhanced by their possible applications in spintronic devices. Furthermore, in recent years much of the search for variable room temperature magnetic refrigerants has focused on low-cost transition metal-rich compounds such as MnAs [8] and MnFe (P, As) [9], which present a significant magnetocaloric effect [10, 11]. Superconductivity was not considered possible in manganese-based compounds due to the strong magnetism of Mn. However, very recently the discovery of pressure-induced superconductivity in MnP attracted much attention due to its unconventional pairing mechanism [12]. MnP is the first manganese-based superconductor uncovered among the Mn-based compounds, which was achieved via the application of high pressure.

Transition metal monophosphides TP (T = Cr, Mn, Fe, and Co) crystallize into *Pnma* structure at ambient conditions [13]. Definition of the orthorhombic axes in MnP-type structures is ambiguous in the literature. The axis convention $c > a > b$ is used in this investigation. Figure 1 shows that both lattice parameters a and c decrease as the ionic radius shrinks. However, the lattice parameter b (space group with *Pnma* setting) of MnP is larger than that of the neighboring transition-metal-based monophosphides at ambient conditions, as shown in figure 1. From a crystallographic viewpoint, MnP is isostructural with CoP, FeP, and CrP, which implies that its novel physical properties under high pressure may originate from these structural characteristics.

From a crystallography perspective, the orthorhombic MnP phase (Space group: *Pnma*, $Z = 4$) is one of the most common TPn-type structures (T = transition metal, Pn = P, As, Sb, Bi). In this phase, each cation is coordinated by Pn anions and these anions are surrounded by T cations. Bulk MnP crystallizes into an orthorhombic *Pnma* structure ($a = 5.258$ Å, $b = 3.172$ Å, and $c = 5.918$ Å) [14–16] under ambient conditions. Six P at four different Mn–P distances surround Mn, forming a distorted octahedron, and its second coordination sphere contains 6 Mn ions with three Mn–Mn distances. In the absence of external magnetic fields, MnP orders ferromagnetically around room temperature, $T_C = 291.5$ K [17], and at low temperatures presents a transition to a screw antiferromagnetic structure (helimagnetic) at $T_N = 47$ K. Such complex magnetism has been explained by spin-wave theory [18, 19] and was more recently ascribed to the influence of magnetocrystalline anisotropy [16].

Previous investigations on unconventional superconductors suggested that external pressure remarkably adjusts their crystal and magnetic structures, consequently tailoring their physical behaviors such as the appearance of superconductivity [2, 20–23]. Banus studied the magnetic behavior of MnP under high pressure [24] and the experimental results indicated that the Curie temperature (T_C) decreased with pressure with $\Delta T_C/\Delta P = -18.5$ K GPa^{-1} (0–2 GPa) and -25 K GPa^{-1} (2–3 GPa). As the pressure further increased, a pressure-induced ferromagnetic to antiferromagnetic transformation occurred. However, Banus's experimental pressure range only covered 5 GPa. A recent investigation on magnetic and electrical transport properties indicated that a high-quality single crystal MnP sample became superconducting below ~1 K when its long-range magnetic order was just suppressed by the application of high pressure of ~8 GPa [12]. Very recently, the evolution of magnetic properties of MnP as a function of temperature and pressure has been investigated with neutron diffraction and muon-spin rotation methods [25, 26]. The subsequent phase diagram of MnP featured a domelike superconducting phase after a gradual pressure-induced suppression of the magnetic phase. This is reminiscent of the phase diagrams of cuprates, heavy fermions, iron- and chromium-based superconductors [2, 27].

In crystal chemistry, the MnP-type phase is fundamentally important for investigating structural transformations. The structure for *Pnma* phase of MnP is an extensively existed parent structure being a so-called prototype. Extensive experimental and theoretical work has been devoted to studying the MnP-type ↔ NiAs-type phase transition [28], since the MnP-type structure is one of the most common prototypes distorted from a NiAs-type. Although MnP is a very important prototype of the TPn-type compounds, previous experimental x-ray diffraction (XRD) investigations on its structural evolution behavior under high pressure are scant. In order to understand the comprehensive physical properties of MnP, knowledge of its crystal structure under high pressure is indispensable. Therefore, we investigated the crystallographic structural evolution of MnP under high pressure using angle-dispersive synchrotron x-ray diffraction (AD-XRD) and density functional theory (DFT) calculations in this study. Notably, the prototype MnP undergoes a remarkable pressure-induced structural phase transition, which sheds light on the of B31 prototype structure. This finding provides crystallographic support for the interpretation of TPn physical properties.

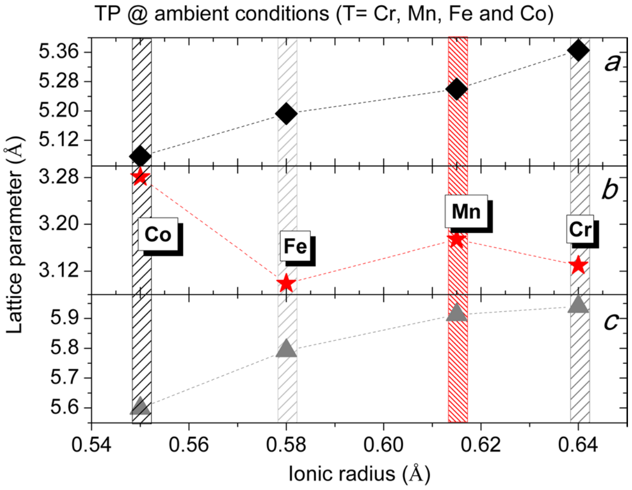

Figure 1. Lattice parameters of TP (T = Cr, Mn, Fe, and Co) at ambient conditions as a function of the ionic radius.

2. Experimental and theoretical details

In this work, MnP single crystals were grown using the Sn-flux method and ground in a mortar to obtain the fine powder sample used for our high-pressure AD-XRD experiment. The phase quality of the sample used in this work was confirmed using synchrotron XRD measurements at the beamline of 16-BM-D ($\lambda = 0.4246$ Å) at the Advanced Photon Source (APS) at the Argonne National Laboratory (ANL). The high-pressure synchrotron XRD experiment was carried out using a symmetric diamond anvil cell with 400 μm culet. A Re gasket with a thickness of 250 μm and a pre-indentation thickness of 45 μm was used. The 120 μm diameter sample chamber was filled with a mixture of the powder, a ruby chip, and some silicone oil as the pressure-transmitting medium. AD-XRD patterns were taken with a MarCCD detector using synchrotron radiation beams monochromatized to a wavelength of 0.6199 Å at beamline BL15U1 of the Shanghai Synchrotron Radiation Facility (SSRF). Two-dimensional image plate patterns were converted to 1D intensity versus degree data using the Fit2D software package [29]. The experimental pressures were determined by the pressure-induced fluorescence shift of ruby [30]. The XRD patterns were analyzed with Rietveld refinement using the GSAS program package [31] with an EXPGUI user interface [32].

The prediction of the MnP crystal structure under high pressures was performed with the *ab initio* random structure searching techniques (AIRSS) code [33, 34] and chemical formula numbers varying from 4 to 8. Structural optimization and electronic structure calculations were performed in the framework of DFT through projector-augmented wave (PAW) method as implemented in the Vienna *ab initio* simulation package (VASP) code [35, 36]. The exchange and correlation functional was treated by generalized gradient approximation with Perdew–Burke–Ernzerhof (GGA-PBE) [37]. The cutoff for plane wave basis of 500 eV and a *k*-point grid with a spacing of $0.03 \times 2\ \pi$/Å in the Monkhorst Pack scheme for integration in the Brillouin zone were tested to ensure the convergence of the total force for each atom was within 1×10^{-3} eV Å^{-1}. The phonon spectrum calculations were performed through supercell approach, as implemented in Phonopy code [38]. A $2 \times 2 \times 2$ supercell was used for the *Pnma* phase and a $3 \times 3 \times 3$ supercell was used for the $P2_13$ and *Pm*-3*m* phase during phonon calculations.

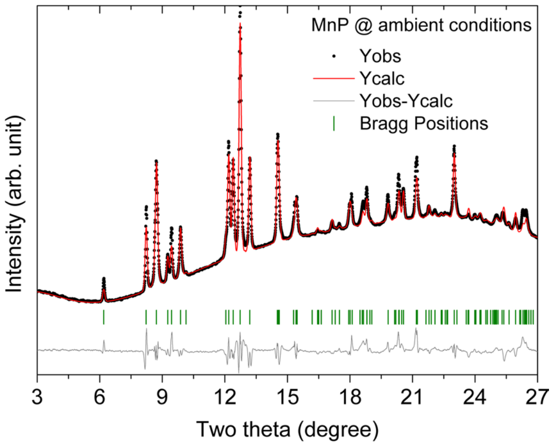

Figure 2. Rietveld refinement of the synchrotron XRD ($\lambda = 0.4246$ Å) profiles for MnP. The solid spheres are the observed data and the solid lines are the calculated diffraction patterns. The positions of the space group allowed reflections are indicated with solid vertical short lines.

3. Experimental and theoretical Results

To begin with, the phase quality of the samples in the present study was checked by XRD technique. Figure 2 shows the final refinement of the MnP diffraction pattern at ambient conditions, collected at the 16 BM-D beamline of APS at ANL using the *Pnma* model from [17]. Figure 2 shows that the sample we used was well prepared without other detectable impurities.

3.1. High-pressure AD-XRD patterns of MnP

Figure 3(a) demonstrates selected patterns of the MnP AD-XRD results under various pressures. For comparison, the Bragg diffraction of the *Pnma* phase is marked at the bottom of figure 3(a). The compressibility of the *b*-axis is much larger than those of the *a*- and *c*-axes according to a previous investigation on 3*d* transition metal pnictides [20]. MnP is a prototype crystal structure of these 3*d* transition metal pnictides. Therefore, the compressibility of the *Pnma* phase of MnP may follow their analogous compressibility behavior. Based on these considerations, the XRD patterns (lower diffraction angle) of the MnP *Pnma* phase were classified by group as shown in figure 3(b).

The diffraction peaks correlating to the *a*- and *c*-axes are represented by red dashed lines, while those dependent on the *b*-axis are marked with blue dashed lines. Figure 3(b) shows that the slope of red line is clearly smaller than those of the blue lines, which indicates that the compressibility of the *b*-axis is much larger than those of the *a*- and *c*-axes. This phenomenon is analyzed in the subsequent section. The (0 1 1) diffraction peak is on the left of (2 0 1) and (1 0 2) for MnP *Pnma* phase

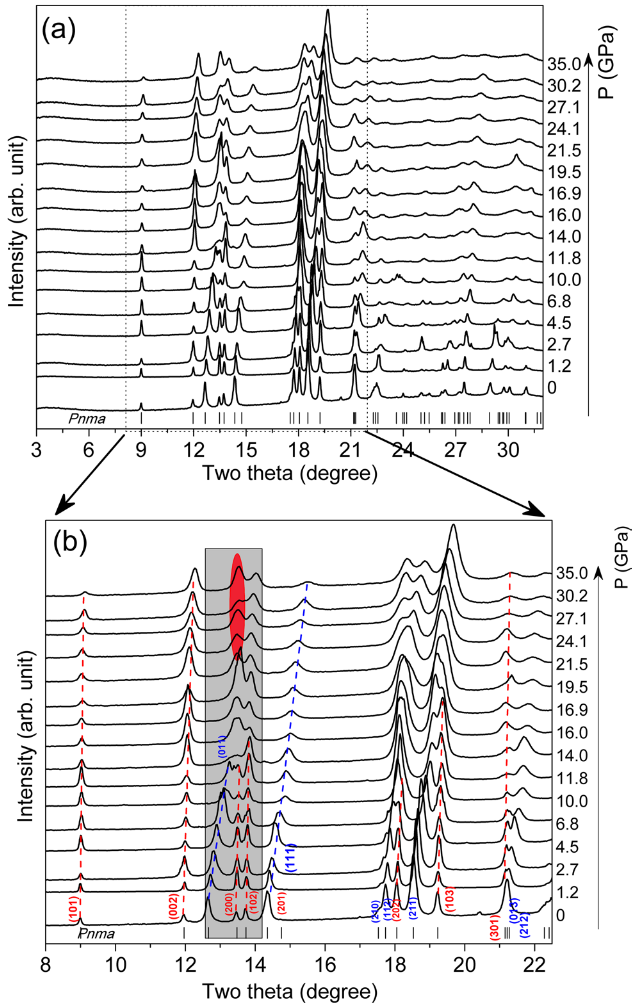

Figure 3. (a) Angle dispersive XRD ($\lambda = 0.6199$ Å) patterns of MnP under selected pressures at room temperature. Indicated pressures were measured using the ruby fluorescence gauge. The Bragg diffraction peak of the *Pnma* phase for MnP is marked with short vertical lines. (b) Fractional Angle dispersive XRD patterns of MnP in (a), red and blue dashed lines is visual aid for classifying the diffraction peaks.

at ambient conditions. Based on the aforementioned (0 1 1), (2 0 1) and (1 0 2) difference slope, it is remarkably to expect that the diffraction peak of (0 1 1) will merge with those of (2 0 1) and (1 0 2) because (0 1 1) moves faster than those of (2 0 1) and (1 0 2) as the pressure increases (see rectangular region of figure 3(b)). As the pressure further increases, new diffraction peaks appear as labeled by the elliptical region of figure 3(b). This suggests a pressure-induced structural phase transition (*Pnma* → high-pressure phase (Phase II)) occurs in MnP around 15 GPa. Finally, the pressure was released to the atmospheric pressure to check the reversibility of the pressure-induced structural phase transition of MnP. All of the diffraction peaks could be indexed to a *Pnma* structure when the pressure was released, as shown in figure 4. The overlapping and the variation of the diffraction peaks' relative intensity obtained under decompression process was observed compared to the ambient XRD pattern, which was collected while increasing pressure. This finding confirmed that the pressure-induced structural phase transition of MnP is reversible.

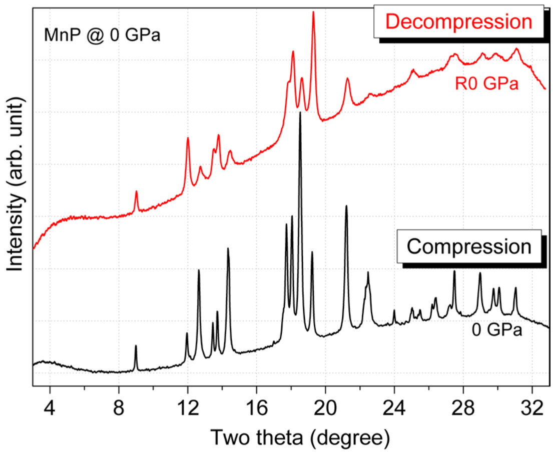

Figure 4. The comparison of XRD patterns taken under compression and decompression cycles.

3.2. Polymorphism of MnP under high pressure investigated by DFT

Gibb's energy is minimized when a system reaches equilibrium at constant temperature and pressure, and is treated as a convenient criterion of stability under given conditions. In ground state condition, Gibb's energy degenerates to enthalpy as the temperature is 0 K. The ground state stability for *Pnma* phase MnP was verified by the present DFT calculation (see figure 5(a)). Our structure searches produced several candidates for the high-pressure phases and the enthalpy difference under high pressure for MnP is summarized in figure 5(b). It is very complex to consider various magnetisms during structural optimization. To simplify the question, we assume that the magnetic order is totally suppressed under very high pressure, and treated the high-pressure phase as a paramagnetic material.

It seems there is a structural phase transition from *Pnma* to *Phase* II at around 15 GPa, but the enthalpy difference is so small that almost beyond the accuracy of DFT [39, 40]. Therefore we did not present this DFT results here. Upon compression, a $P2_13$-type MnP (SG no. 198) was energetically preferred above 55 GPa, and the neighbor number of Mn increased from six (in *Pnma* phase) to seven. It is interesting to note that as the pressure increased further, the $P2_13$-type transformed into a CsCl-type (SG Pm-$3m$, no. 221) above 92 GPa, and with the neighbor number increased to eight.

Dynamical stability of the $P2_13$ and Pm-$3m$ structure under high pressure is investigated by calculating the phonon dispersions, shown in figures 5(c) and (d). These calculations confirm that these two structures are dynamically stable at 60 and 90 GPa, respectively. It can be seen from figure 5(d) that Pm-$3m$ phase was dynamically stable during 60 to 150 GPa. The frequency of vibrational mode (such as M point) rises with increasing pressure. We optimized these two structures with Mn atom ferromagnetic configurations and found the magnetization quenched to zero at high pressure. As shown in the band structures in figure 6, based on the GGA-PBE functional, the $P2_13$-type MnP at 60 GPa seems to be a semiconductor with an indirect band gap of 0.35 eV, while the Pm-$3m$-type MnP at 90 GPa is metal. Hubbard U might slightly change the

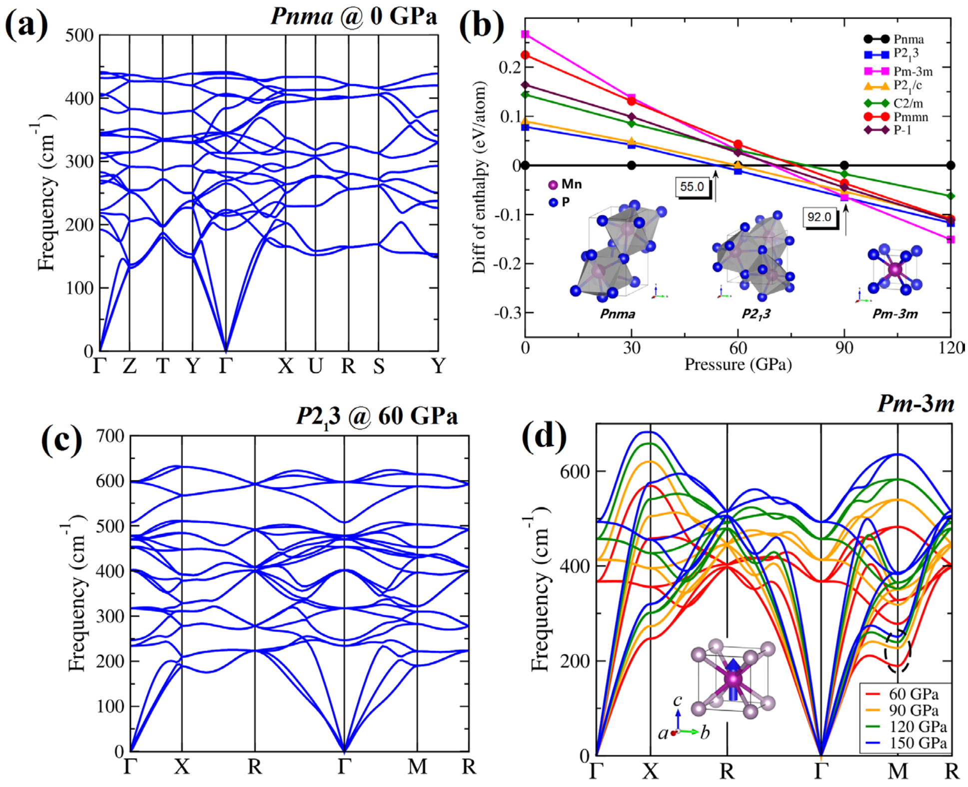

Figure 5. (a) Phonon dispersion for the *Pnma* phases of MnP under 0 GPa. (b) Enthalpy difference (Relative to *Pnma* phase) as a function of pressure for MnP. The inset shows schematic representations of the *Pnma*, $P2_13$ *and Pm-3m* phase, respectively. Phonon dispersions for the high-pressure phases of MnP, the $P2_13$ phase at 60 GPa (c) and the *Pm-3m* phase at 60, 90, 120 and150 GPa, respectively (d).

values of the band gap, but this is not the main subject of our work here.

4. Discussion

4.1. The polymorphism of TP (T = Ti, V, Cr, Mn, Fe, Co and Ni) under ambient conditions and high-pressure application

As reflected in figure 7(a), the transition metal phosphides TP (T = Ti, V, Cr, Mn, Fe, Co and Ni) crystallize into $P6_3/mmc$ (T = Ti and V), *Pnma* (T = Cr, Mn, Fe and Co) and *Pbca* (T = Ni) structures at ambient conditions, respectively. It is interesting to note that TP (T = Ti ~ Co) transformed from $P6_3/mmc$- to *Pnma*-type as the ionic radius decreases (or atomic number increased). The decrease of ionic radii resulted in the enhancement of inner chemical pressure. *Pnma*-type is one of the structures distorted from $P6_3/mmc$-type. Therefore, we performed GSAS refinement fitting of XRD data for MnP above ~15 GPa using $P6_3/mmc$-type. However, the NiAs ($P6_3/mmc$)-type structure did not match the Phase II XRD pattern collected beyond 15.4 GPa, which is consistent with reported data [41]. Since NiP is one of the isomorphous compounds with MnP, it is natural to assume that MnP adopts a NiP-type structure under high pressure. However, the diffraction peak positions of the NiP-type phase (space group: *Pbca*) failed to match our HP phase of MnP. The maximal subgroup of *Pnma* is $P2_1/m$ (No. 11), $P2_1/c$ (No. 14), $P2_12_12_1$ (No. 19), $Pmc2_1$ (No. 26), $Pmn2_1$ (No. 31), and $Pna2_1$ (No. 33). In addition, the possible high-pressure polymorphism of MnP performed with the AIRSS method is also compared with the experimental results shown in figure 7(b). From figure 7(b) we found that the simulated XRD obtained from the above mentioned crystal structure model was an unsatisfactory match with our experimental results.

4.2. Pressure-induced structural phase transition in MnPn (Pn = P, As and Sb)

Nitrogen (N), as the first V group elements that can be experimentally used to synthesize various transition metal mononitrides, has been studied for decades because of the variety of its mechanical, electrical and magnetic properties [42, 43]. For MnN, the stoichiometry ratio for Mn and N is not 1:1 due to the nitrogen vacancies, resulting in an incomplete understanding of its crystal structure [44, 45]. Thus, the variation of the MnN crystal structure under high pressure is not included in the present work. The structural variations of MnPn have been studied previously. Figure 8 summarizes the phase diagram of MnPn (Pn = P, As and Sb) under room temperature with increasing pressure, reported in the literature, i.e. MnAs [46], MnSb [47]. $MnAs_{0.80}Sb_{0.20}$ [48], and $MnAs_{0.88}P_{0.12}$ [49]. From figure 8 we found the transition pressure ($B8_1 \rightarrow B31$) for MnAs and MnSb and its solutions ($MnAs_{0.80}Sb_{0.20}$) were ~0.4, ~4 and ~11 GPa, respectively. The transition pressure ($B8_1 \rightarrow B31$) increases as the radius of the anions increases (As, 1.19 Å; Sb, 1.40 Å [50]). Generally, isostructural compounds containing different cations will undergo similar phase transitions at progressively lower pressures as the cation radii increase. However, the cation radii as a function of the

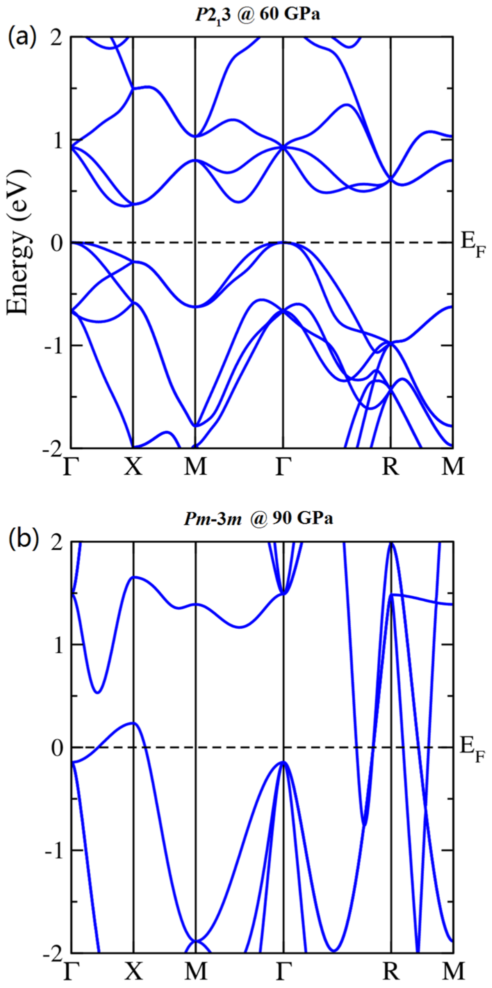

Figure 6. Calculated electronic band structures of MnP in (a) $P2_13$ phase at 60 GPa and (b) Pm-$3m$ phase at 90 GPa. Based on the GGA-PBE functional, the $P2_13$ MnP seems to be a semiconductor with an indirect band gap of 0.35 eV, while Pm-$3m$-MnP is metal.

phase transition pressure in MnAs and MnSb and its solutions ($MnAs_{0.80}Sb_{0.20}$) did not follow this empirical rule. Cooling and compression exhibited a similar effect on shrinking the volume of material. For example, decreasing temperature and increasing pressure resulted in a cubic (Fm-$3m$)-to-orthorhombic (*Pnma*) structural phase transition in CrN at ~282 K and ~1 GPa, respectively [51]. However, it was shown that MnAs undergoes a structural phase transition of NiAs-type → MnP-type at 315 K (warming) and 0.4 GPa (compression), respectively [52, 53]. The mechanism of this anomalous structural phase transition deserves further studies. However, the phosphorus-doped MnAs ($MnAs_{0.88}P_{0.12}$) crystallizes into a *Pnma* structure and is stable up to 30 GPa.

4.3. The comparison of CrAs and MnP under high pressure

CrAs and MnP recently has attracted much attention as important model systems for studying the interplay between magnetism and superconductivity in unconventional superconductors. CrAs and MnP crystallize into a *Pnma* structure at ambient conditions, and exhibit comparable lattice parameters to CrAs ($a = 5.583$ Å, $b = 3.575$ Å and $c = 6.113$ Å, experimental) [20] and MnP ($a = 5.258$ Å, $b = 3.172$ Å and $c = 5.918$ Å, obtained from this synchrotron XRD data). Superconductivity was discovered near long-range magnetic order in CrAs and MnP via the application of high pressure. However, the critical pressures (P_c) of superconductivity in CrAs and MnP have a large difference with $P_c \approx 0.4$ and 8 GPa, respectively. The close proximity of superconductivity to pressure-induced magnetic instability in CrAs and MnP suggests an unconventional pairing mechanism, perhaps driven by the quantum-critical spin fluctuations. Although CrAs and MnP adopt the same orthorhombic structure and possess a superconducting state under pressure, the dominating magnetic interaction in CrAs and MnP exhibits a remarkable difference. CrAs and MnP possess a first-order and second-order magnetic phase transition, respectively. This may be a factor in their vastly different critical pressures. The bulk superconductivity of CrAs emerges at the critical pressure of 0.4 GPa, where the first-order antiferromagnetic transition at $T_N = 265$ K under ambient pressure is completely suppressed. In comparison to CrAs, MnP possesses a more complicated phase diagram of temperature and pressure. The present AD-XRD evidenced a pressure-induced structural phase transition in MnP ~ 15 GPa. However, for CrAs, our AD-XRD measurement shows that orthorhombic CrAs exhibits crystallographic symmetry variation up to 30 GPa (these results will be published elsewhere). This comparison suggests that CrAs and MnP exhibit different crystal and magnetic behaviors under high pressure.

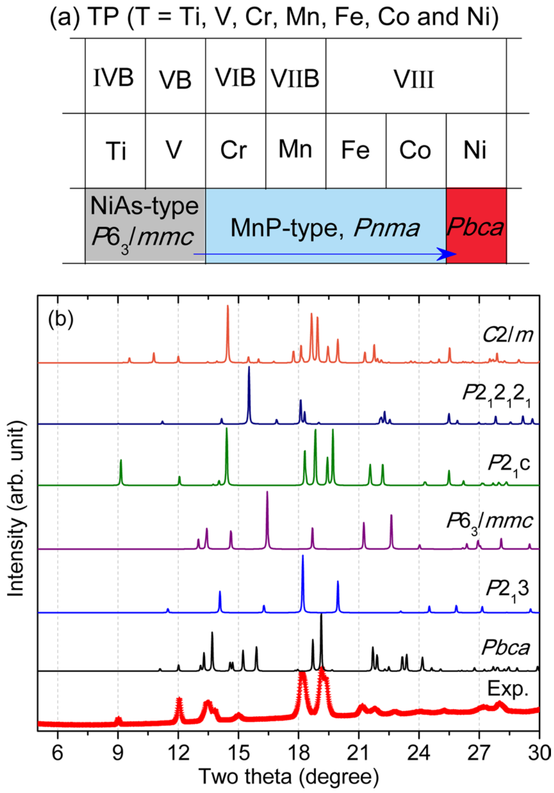
(a) TP (T = Ti, V, Cr, Mn, Fe, Co and Ni)

IVB	VB	VIB	VIIB	VIII		
Ti	V	Cr	Mn	Fe	Co	Ni
NiAs-type $P6_3/mmc$		MnP-type, *Pnma*				*Pbca*

Figure 7. (a) Schematic crystallographic phase of TP (T = Ti, V, Cr, Mn, Fe, Co and Ni) under ambient conditions. (b) The comparisons of experimental and simulated XRD patterns of MnP with different polymorphism under high pressure ~15 GPa.

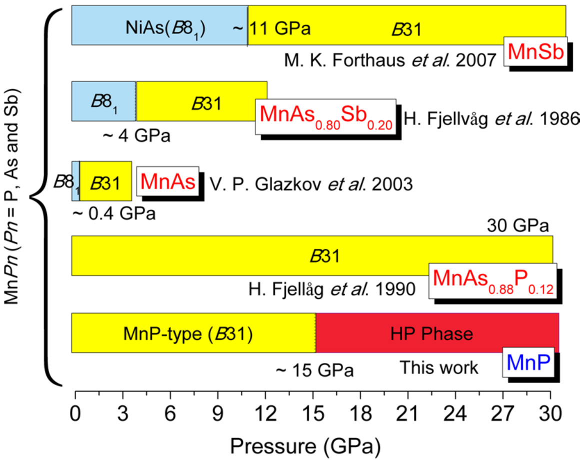

Figure 8. Phase diagram of MnPn (Pn = P, As and Sb) under room temperature with increasing pressure referred from adapted literature.

5. Conclusions

We investigated the high-pressure phase transition in MnP by synchrotron powder XRD. The crystal structure of MnP between 0 to 15 GPa was stable. However, the compressibility of the *b*-axis was much larger than those of the *a*- and *c*-axes. As the pressure increased, the *Pnma* phase (Phase I) transformed into a high-pressure phase (Phase II). The high-pressure phase recovered to a *Pnma* phase after pressure was released. We suggested that the occurrence of superconductivity in MnP was induced by suppression of the long-range antiferromagnetically ordered state using applied pressure rather than a macro crystallographic variation (structural phase transition). The polymorphism of transition metal phosphides was summarized and attempted to match the phase II of MnP. With our extensive crystal structure searching and *ab initio* calculations, we predict that MnP underwent two pressure-induced structural phase transitions of $Pnma \rightarrow P2_13$ and $P2_13 \rightarrow Pm\text{-}3m$ (CsCl-type) at 55.0 and 92.0 GPa, respectively. The tendency of pressure-induced structural phase transition in MnPn was analyzed. In addition, pressure-induced structural phase transition in manganese monophosphides as well as comparison of CrAs and MnP under high pressure was discussed.

Acknowledgments

The authors acknowledge the support of NSAF (Grant No: U1530402) and Science Challenging Program (Grant No. JCKY2016212A501). J S thanks the financial support from the MOST of China (Grant Nos. 2016YFA0300404, 2015CB921202), the NSFC (Grant Nos: 51372112, 11574133), NSF Jiangsu province (No. BK20150012), the Fundamental Research Funds for the Central Universities and Special Program for Applied Research on Super Computation of the NSFC-Guangdong Joint Fund (the 2nd phase). JGC is supported by the National Science Foundation of China (Grant No. 11574377). Part of the calculations was performed on the supercomputer in the High Performance Computing Center of Nanjing University and 'Tianhe-2' in NSCC-Guangzhou. Portions of this work were performed at the BL15U1 beamline, Shanghai Synchrotron Radiation Facility (SSRF) in China. The authors would like to thank SSRF for use of the synchrotron radiation facilities. Use of NSLS is supported by the US Department of Energy (DOE), Office of Science, Office of Basic Energy Sciences, under Contract DEAC02-98CH10886. Beamline X17 of NSLS is supported by the Consortium for Materials Properties Research in Earth Sciences (COMPRES). The HPCAT facility is supported by CIW, CDAC, UNLV and LLNL through funding from DOE-NNSA, DOE-BES and NSF. APS is supported by DOE-BES, under Contract No. DE-AC02-06CH11357.

References

[1] Kamihara Y, Watanabe T, Hirano M and Hosono H 2008 *J. Am. Chem. Soc.* **130** 3296
[2] Wu W, Cheng J-G, Matsubayashi K, Kong P P, Lin F K, Jin C Q, Wang N L, Uwatoko Y and Luo J L 2014 *Nat. Commun.* **5** 5508
[3] Kotegawa H, Nakahara S, Tou H and Sugawara H 2014 *J. Phys. Soc. Japan* **83** 093702
[4] Hagg G 1929 *Nova Acta Regiae Soc. Sci. Upsaliensis* **7** 95
[5] Fylking K-E and Arkiv K 1935 *Mineral. Geol.* **11** 48
[6] Shapira Y, Becerra C C, Oliveira N F Jr and Chang T S 1981 *Phys. Rev.* B **24** 2780
[7] Matsumura Y, Narita E and Hirahara E 1975 *J. Phys. Soc. Japan* **38** 1264
[8] Wada H and Tanabe Y 1979 *Appl. Phys. Lett.* **79** 3302
[9] Tegus O, Bruck E, Buschow K H and de Boer F R 2002 *Nature* **415** 150
[10] Gercsi Z and Sandeman K G 2010 *Phys. Rev.* B **81** 224426
[11] Guillou F and Brück E J 2013 *J. Appl. Phys.* **114** 143903
[12] Cheng J-G, Matsubayashi K, Wu W, Sun J P, Lin F K, Luo J L and Uwatoko Y 2015 *Phys. Rev. Lett.* **114** 117001
[13] Rundqvist S 1962 *Acta Chem. Scand.* **16** 287
[14] Rundqvist S and Nawapong P C 1965 *Acta Chem. Scand.* **19** 1006
[15] Zieba A, Becerra C C, Fjellvag H, Oliveira N F and Kjekshus A 1992 *Phys. Rev.* B **46** 3380
[16] Reis M S, Rubinger R M, Sobolev N A, Valente M A, Yamada K, Sato K, Todate Y, Bouravleuv A, von Ranke P J and Gama S 2008 *Phys. Rev.* B **77** 104439
[17] Huber E E Jr and Ridgley D H 1964 *Phys. Rev.* **135** A1033
[18] Takase A and Kasuya T 1979 *J. Phys. Soc. Japan* **47** 491
[19] Todate Y, Yamasa K, Endoh Y and Ishukawa Y 1987 *J. Phys. Soc. Japan* **56** 36
[20] Yu Z H, Wu W, Hu Q Y, Zhao J G, Li C Y, Yang K, Cheng J G, Luo J L, Wang L and Mao H K 2015 *Proc. Natl Acad. Sci. USA* **112** 14766
[21] Shen Y *et al* 2016 *Phys. Rev.* B **93** 060503
[22] Uhoya W, Tsoi G, Vohra Y K, McGuire M A, Sefat A S, Sales B C, Mandrus D and Weir S T 2010 *J. Phys.: Condens. Matter* **22** 292202
[23] Yu Z H *et al* 2014 *Sci. Rep.* **4** 7172
[24] Banus M D 1972 *J. Solid State Chem.* **4** 391
[25] Matsuda M *et al* 2016 *Phys. Rev.* B **93** 100405
[26] Khasanov R, Amato A, Bonfà P, Guguchia Z, Luetkens H, Morenzoni E, De Renzi R and Zhigadlo N D 2016 *Phys. Rev.* B **93** 180509
[27] Sachdev S and Keimer B 2011 *Phys. Today* **64** 29
[28] Franzen H F, Haas C and Jellinek F 1974 *Phys. Rev.* B **10** 1248
[29] Hammersley A, Svensson S, Hanfland M, Fitch A and Hausermann D 1996 *High Press. Res.* **14** 235
[30] Mao H K, Xu J A and Bell P 1986 *J. Geophys. Res.* **91** 4673
[31] Larson A C and Von Dreele R B 1994 *Los Alamos National Laboratory Report LAUR* 86-748

[32] Toby B H 2001 *J. Appl. Cryst.* **34** 210

[33] Pickard C J and Needs R J 2006 *Phys. Rev. Lett.* **97** 045504

[34] Pickard C J and Needs R J 2011 *J. Phys.: Condens. Matter* **23** 053201

[35] Hohenberg P and Kohn W 1964 *Phys. Rev.* **136** B864

[36] Kresse G and Furthmüller J 1996 *Comput. Mater. Sci.* **6** 15

[37] Perdew J P, Burke K and Ernzerhof M 1996 *Phys. Rev. Lett.* **77** 3865

[38] Togo A, Oba F and Tanaka I 2008 *Phys. Rev.* B **78** 134106

[39] Karki B B, Warren M C, Stixrude L, Ackland G J and Crain J 1997 *Phys. Rev.* B **55** 3465

[40] Gupta S D and Jha P K 2014 *Earth Planet Sci. Lett.* **401** 31

[41] Wang Y S, Feng Y J, Cheng J-G, Wu W, Luo J L and Rosenbaum T F 2016 *Nat. Commun.* **7** 13037

[42] Kaner R B, Giman J J and Tolbert S H 2005 *Science* **308** 1268

[43] Tong W P, Tao N R, Wang Z B, Lu J and Lu K 2003 *Science* **299** 686

[44] Suzuki K, Kaneko T, Yoshida H, Obi Y, Fujimori H and Morita H 2000 *J. Alloys Compd.* **306** 66

[45] Miao M S and Lambrecht Walter R L 2007 *Phys. Rev.* B **76** 195209

[46] Glazkov V P, Kozlenko D P, Podurets K M, Savenko B N and Somenkov V A 2003 *Crystallogr. Rep.* **48** 54

[47] http://hasyweb.desy.de/science/annual_reports/2007_report/part1/contrib/42/22084.

[48] Fjellvåg H, Hochheimer H D and Hönle W 1986 *Phys. Lett.* A **118** 293

[49] Fjellvåg H, Stølen S, Grosshans W A and Krüger T 1990 *J. Solid State Chem.* **87** 222

[50] Slater J C 1964 *J. Chem. Phys.* **41** 3199

[51] Rivadulla F *et al* 2009 *Nat. Mater.* **8** 947

[52] Wilson R H and Kasper J S 1964 *Acta Cryst.* **17** 95

[53] Łażewski J, Piekarz P, Toboła J, Wiendlocha B, Jochym P T, Sternik M and Parlinski K 2010 *Phys. Rev. Lett.* **104** 147205